5-2022

Synthesis, Structural Characterization, and in vitro Biological Assessment of trans- Platinum (II) Thionate Complexes as Potent Anticancer Agents

Mia Alshami

Synthesis, Structural Characterization, and in vitro Biological Assessment of trans-Platinum (II) Thionate Complexes as Potent Anticancer Agents

An Honors Thesis submitted in partial fulfillment of
the requirements for Honors Studies in Chemistry

By

Mia Alshami

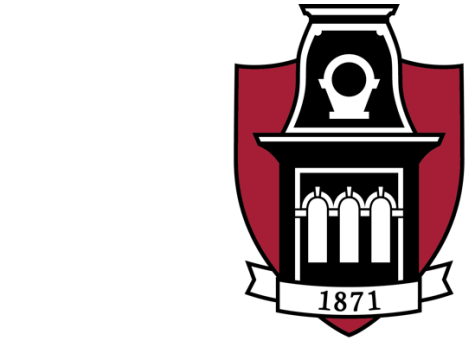

UNIVERSITY OF
ARKANSAS

Spring 2022

Department of Chemistry and Biochemistry

J. William Fulbright College of Arts and Sciences

The University of Arkansas

Acknowledgements

First, I would like to thank the University of Arkansas Honors College and the Arkansas Department of Higher Education for providing me with grants to fund my research efforts. Thank you to Dr. Hudson Beyzavi for giving me the opportunity to work in his laboratory for three years and to contribute to two published papers throughout my time working in his research lab. Thank you to Dr. Matt McIntosh for guiding me through the thesis writing process and allowing me to pursue my research interests. Thank you to Dr. Adnan Ali Khalaf Alrubaye, Dr. Neil Allison and Dr. Joshua Sakon for graciously sharing their time to review and critique my thesis.

Thesis Committee Members:

Dr. Matt McIntosh, Chair

Dr. Adnan Ali Khalaf Alrubaye

Dr. Neil Allison

Dr. Joshua Sakon

Table of Contents

Abstract

The content of this thesis has been originally reported in our published paper, "*trans*-Platinum (II) Thionate Complexes: Synthesis, Structural Characterization, and in vitro Biological Assessment as Potent Anticancer Agents" *ChemPlusChem* **2019** 84, 1525-1535, DOI: 10.1002/cplu.201900394, in which I served as coauthor. Cancer caused 9.6 million deaths in 2018 worldwide, with 18.1 million new diagnoses during that same year. The most widely used metal in anticancer drugs is platinum (Pt), and these drugs are used to treat almost 50% of cancer patients. To optimize drug effectiveness, *trans*-configured Pt(II) complexes have been introduced as a strategy to potentially overcome the drawbacks that *cis*-configured Pt(II) have. Also, *trans*-configured Pt(II) complexes may diminish severe side effects, drug resistance, poor selectivity, and serious toxicity of cisplatin. A series of Pt(II) complexes *trans*-[Pt(PPh_2allyl)$_2$(k^1-S-SR)$_2$], **1,** PPh_2allyl = allyldiphenylphosphine, SR = pyridine-2-thiol (Spy, **1a**), 5-(trifluoromethyl)-pyridine-2-thiol (SpyCF_3-5, **1b**), pyrimidine-2-thiol (SpyN, **1c**), benzothiazole-2-thiol (Sbt, **1d**), benzimidazole-2-thiol (Sbi, **1e**), were synthesized. They were characterized by NMR, HR ESI-MS and X-ray crystallography. These complexes were treated by human cancer cell lines (A549, SKOV3, MCF-7) and shown the promising antitumor effects in comparison with cisplatin. These compounds were showed suitable selectivity between tumorigenic and non-tumorigenic (MCF-10A) cell lines. Analyses of cell cycle progression and apoptosis were conducted for **1a,** the best cytotoxic compound, to screen dose/time response and to study the effects of the antiproliferative mechanism. The electrophoresis mobility shift assay was performed to assess the direct interaction of **1a** with DNA and the strong genotoxic ability was indicated through comet assay method.

Publications and Grants

Honors College Research Grant. Design, Synthesis, and Characterization of Novel Heterobimetallic Pt^{II}–M^{III} (M = Ir, Rh) Complexes as Potent Anticancer Agents. Awarded January 2021 in the amount of $4,000, supervised by Dr. Beyzavi and Dr. McIntosh.

J. Hu, M. Nikarvesh, H.R. Shahsavari, R. Babadi Aghakhanpour, A.L. Rhiengold, **M. Alshami**, Y. Sakamaki, and M.H. Beyzavi. "A C^N Cycloplatinated (II) Fluorido Complex: Csp^3-F Bond Formation and Photophysical Studies." *Inorganic* Chemistry **2020**, 59, 16319-16327.

Y. Sakamaki, H. A. Mirsadeghi, M. Fereidoonnezhad, F. Mirzaei, Z. M. Dehkordi, S. Chamyani, **M. Alshami**, S. Abedanzadeh, H. R. Shahsavari, and M. H. Beyzavi. "Synthesis, Structural Characterization and in Vitro Biological Assessment of Trans-Platinum(II) Thionate Complexes as Potent Anticancer Agents" *ChemPlusChem* **2019,** 84, 1525-1535. DOI: 10.1002/cplu.201900394.

Student Undergraduate Research Fund. Pt(II)-Au(I) Heterometallic Complexes as Anticancer Drugs. Awarded February 2020 in the amount of $4000, supervised by Dr. Beyzavi.

Introduction and Background

Cancer caused 9.6 million deaths in 2018 worldwide, with 18.1 million new diagnoses during that same year. This makes cancer the second most frequent disease after cardiovascular disease. One in 5 men and one in 6 women worldwide will develop cancer during their lifetime, and one in 8 men and one in 11 women will die from the disease.[1] Chemotherapy involves giving one or more cytotoxic drugs including metal-based drugs. The most widely used metal in these drugs is platinum (Pt). Pt anticancer agents are used to treat almost 50% of cancer patients. There are three main Pt-based drugs that are used throughout the world for the treatment of cancer: cisplatin, carboplatin, and oxaliplatin (Fig. 1).[2]

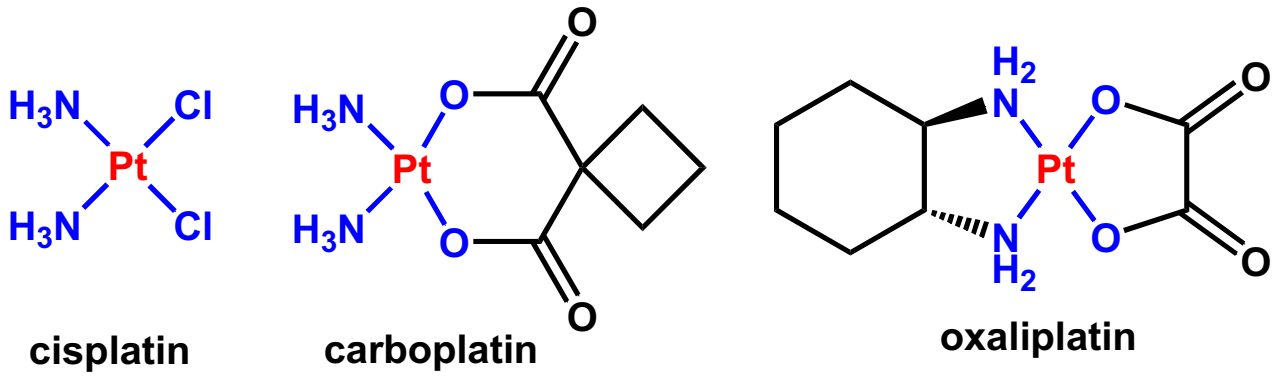

Figure 1. *Pt-based chemotherapy drugs.*[2]

Cisplatin is currently the leading metal-based antitumor drug in the field because of its effective activities against several human malignancies. However, cisplatin has major limitations in its clinical applications such as several side effects, drug resistance, and severe toxicity.[3] Therefore, there have been several continuous efforts to create new structures of platinum-based anticancer agents that have an improved therapeutic index.

Understanding the Coordination Complex

To design a potent metal-based therapeutic complex, it is essential to know what happens to the coordination complex under physiological conditions. Deoxyribonucleic acid (DNA) is considered the major pharmacological target for cisplatin and the other platinum-based anticancer complexes.[4] Furthermore, the biological effectiveness of platinum complexes is derived from the formation of drug-DNA cross-link adducts, which has been widely studied.[5] Platinum anticancer complexes coordinatively interact with DNA bases at the N^7 positions of Guanine and Adenine residues, which then generate DNA lesions and ultimately cause cell death. The kinetic and thermodynamic interactions between these platinum(II) complexes and DNA have been widely investigated.[6] The activity and toxicity of platinum drugs are both directly attributed to the nature of the ligand around the Pt center, particularly the kinetics of exchange reactions.[7]

To optimize drug effectiveness, *trans*-configured Pt(II) complexes have been introduced as a strategy to potentially overcome the drawbacks that *cis*-configured Pt(II) have. Also, *trans*-configured Pt(II) complexes may diminish the severe side effects, drug resistance, poor selectivity, and serious toxicity of cisplatin.[8] *Trans*-configured Pt(II) complexes have displayed considerable *in vitro* antiproliferative effects against a wide range of cancer cells.[9] These platinum complexes are unique in that they have bulky planar ligands, which results in different structural and DNA-binding properties in comparison with cisplatin analogues.[10] In theory, sterically hindered Pt(II) should have reduced reactivity in a substitution reaction with all potential targets, such as nucleophiles on DNA, proteins, and small molecules. However, there is some evidence to suggest that the antitumor activities of platinum(II) complexes actually increases in the presence of sterically hindered ligands.[11] These ligands have the ability to impeded the substitution reactions and inhibit the undesired interactions between Pt(II) centers and cellular components before the

platinum drugs bind to target DNA.[12] Heterocyclic bulky ligands can provide appropriate high steric hindrance and subsequently thermodynamic stability that is desired, which will make the metal complex kinetically inert in nature.[13] Aryl groups are able to facilitate transportation across the cell membrane by increasing lipophilicity, which thereby improves tumor uptake of drugs. The structure of metal-ligand complexes as well as ligand structure are thought to be significant parameters for the antitumor activity of metallodrugs.[6]

Using Thionate Ligands

Heterocyclic thiones or thionates are specific structural motives that combine soft and hard ends while also possessing rich coordination chemistry according to the diverse modes of action ends.[14] In an effort to introduce potential antitumor metal-based complexes of new structure, we have designed a class of Pt(II)-phosphane complexes containing heterocyclic thionate ligands. Previous investigations have previously revealed that phosphane ligands would render the platinum complexes more stable in the physiological environment, leading to lower required drug doses and potentially reduced toxicity.[15] Furthermore, the presence of weakly coordinating carbon moieties in the structure of phosphane ligands can donate different steric and electronic properties to the complex, making it capable of new biological features.

The Proposed Complexes

In this study, we describe the reaction of multiple thionate ligands (pyridine-2-thiol, **a**; 5-(trifluoromethyl)-pyridine-2-thiol, **b**; pyrimidine-2-thiol, **c**; benzothiazole-2-thiol, **d**; and benzimidazole-2-thiol, **e**) with starting complex *cis*-[$Pt(PPh_2allyl)_2Cl_2$], **A**, bearing allydiphenylphosphane (PPh_2allyl) ligand.

The preparation of the newly synthesized Pt(II) thionate complexes was confirmed by NMR spectroscopy. Structural information has been extracted by the X-ray crystallographic

method. Thionates, as a source of sulfur donor ligands, coordinated to the platinum center in *trans*-configuration modes. To investigate the antitumor activity of the complexes, the new *trans*-Pt(II) complexes were evaluated against three human cancer cell lines (lung, A549, ovarian, SKOV3, and breast, MCF-7) by means of the MTT assay. Furthermore, the ability of complex **1a** to inhibit the proliferation of MCF-7 was assessed by measuring cell death via induction of apoptosis. Cell cycle analysis was also applied to study the mechanism of antiproliferative effects of **1a.** To predict the genotoxic effect of complexes on MCF-7 cancer cells, comet assay was used. However, the interaction ability of complexes with DNA was investigated by gel mobility-shift analysis as a valuable method.

Methodology

General Procedures and Materials

^{1}H NMR (400 MHz), $^{19}F\{^{1}H\}$ (376.6 MHz), $^{31}P\{^{1}H\}$ NMR (162 MHz) and $^{195}Pt\{^{1}H\}$ (85.6 MHz) spectra were recorded on a Bruker Avance DPX 400 MHz instrument at room temperature. All chemical shifts (δ) are reported in parts per million (ppm) relative to their corresponding external standards ($SiMe_4$ for ^{1}H, $CFCl_3$ for $^{19}F\{^{1}H\}$, 85% H_3PO_4 for $^{31}P\{^{1}H\}$, Na_2PtCl_6 for $^{195}Pt\{^{1}H\}$) and their coupling constants (*J*) have been expressed in Hz. The microanalyses were performed using a vario EL CHNS elemental analyzer. The instrument for HR ESI-Mass measurement was a Shimadzu IT-Tof with an electrospray ionization source, which is part of the Arkansas Statewide Mass Spectrometry Facility. The allyldiphenylphosphane (PPh_2allyl), pyridine-2-thiol (HSpy), 5-(trifluoromethyl)-pyridine-2-thiol ($HSpyCF_3$-5), pyrimidine-2-thiol (HSpyN), benzothiazole-2-thiol (HSBt), benzimidazole-2-thiol (HSBi) and all the other chemicals were purchased from commercial resources. All the reactions were carried out

under Argon atmosphere and in the common solvents and all solvents were purified and dried according to standard procedures.[16] Precursor complexes *cis,trans*-[$PtCl_2(SMe_2)_2$][17] or *cis*-[$PtCl_2(dmso)_2$][18] were synthesized as reported in the literature.

Synthesis of the Complexes

cis-[Pt(PPh2allyl)2Cl2], A

To a solution of *cis*-[$PtCl_2(dmso)_2$] (450 mg, 1.07 mmol) or *cis,trans*-[$PtCl_2(SMe_2)_2$] (418 mg, 1.07 mmol) in CH_2Cl_2 (20 mL), two equivalents of PPh_2allyl (461 μL, 2.14 mmol) was added. The mixture was stirred at room temperature for 3 h and then the solvent was concentrated to small volume (~ 1 mL) under vacuum, and diethyl ether (3 mL) was added to give **A** as a white solid, which was filtered and washed with diethyl ether (3 x 3 mL) and dried. Yield: 669 mg, 87% Elm. Anal. Calcd. for $C_{30}H_{30}Cl_2P_2Pt$ (718.49): C, 50.15; H, 4.21. Found: C, 50.22; H, 4.26. HR ESI-MS(+) m/z Cacld. for $[M - 2Cl]^{2+}$ 323.5731; Found 323.5737. NMR data in $CDCl_3$: δ (^1H) 7.43 (dd, $^3J_{HH}$ = 8.0 Hz, $^3J_{PH}$ = 10.1 Hz, 8H, H°), 7.35 (t, $^3J_{HH}$ = 7.6 Hz, 4H, H^p), 7.18 (t, $^3J_{HH}$ = 8.0 Hz, 8H, H^m), 5.98-5.90 (m, 2H, H^b), 5.09 (d, $^3J_{H^{c\text{-}cis}H^b}$ = 9.7 Hz, 2H, diastereotopic H^c), 4.84 (dd, $^3J_{H^{c\text{-}trans}H^b}$ = 16.6 Hz, $^4J_{H^{c\text{-}trans}H^a}$ = 3.1 Hz, 2H, diastereotopic H^c), 3.32 (dd, $^3J_{HH}$ = 7.6 Hz, $^2J_{PH}$ = 12.3 Hz, $^3J_{PrH}$ = 35.3 Hz, 4H, H^a); δ ($^{31}P\{^1H\}$) 4.6 (s, $^1J_{PtP}$ = 3671 Hz, 2P); δ ($^{195}Pt\{^1H\}$) −4420.1 (t, $^1J_{PtP}$ = 3679 Hz, 1Pt).

trans-[Pt(PPh2allyl)2(k1-S-Spy)2], 1a

Two equimolar amounts of KSpy (21 mg, 0.14 mmol) were dissolved in ethanol (15 mL) and added to a solution of **A** (50 mg, 0.07 mmol) in CH_2Cl_2 (1 mL). The reaction mixture was removed under reduced pressure and the residue was extracted with CH_2Cl_2 (10 mL). The obtained

green solution was filtered through celite, and the filtrate was concentrated to a small volume (~ 1 mL) under vacuum, and *n*-hexane (5 mL) was added to give **1a** as a green solid, which was filtered and washed with *n*-hexane (3 x 3 mL) and dried. Yield: 45 mg, 74%. Elem. Anal. Calcd. for $C_{40}H_{38}N_2P_2PtS_2$ (867.90): C, 55.36; H, 4.41; N, 3.23; S, 7.39. Found: C, 55.48; H, 4.38; N, 3.28; S, 7.48. HR ESI-MS(+) m/z Cacld. for $[M + 2H]^{2+}$ 434.5874; Found 434.5865. NMR data in $CDCl_3$: δ (^{1}H) 7.93 (m, 2H, H^g), 7.62 (m, 8H, H°), 7.40-7.09 (m, 14H, H^d, H^{m}and H^p), 6.80 (t, $^3J_{HH}$ = 7.8 HZ, 2H, H^e), 6.54 (t, $^3J_{HH}$ = 7.4 Hz, 2H, H^f), 5.83-5.71 (m, 2H, H^b), 4.90 (d, $^3J_H$$^{c\text{-}cis}$H^b = 9.4 Hz, 2H, diastereotopic H^c), 4.71 (d, $^3J_H$$^{c\text{-}trans}$H^b = 15.9 Hz, 2H, diastereotopic H^c), 3.38 (m, 4H, H^a); δ (^{31}P{^{1}H}) 10.3 (s, $^1J_{PtP}$ = 2732 Hz, 2P); δ (^{195}Pt{^{1}H}) - 4747.0 (t, $^1J_{PtP}$ = 2737 Hz, 1Pt).

The other new complexes were made similarly using **A** and the appropriate potassium thionate ligands.

trans-[Pt(PPh2allyl)2(k1-S-SpyCF3-5)2], 1b

Yield: 60 mg, 86%. Elem. Anal. Calcd. for $C_{42}H_{36}F_6N_2P_2PtS_2$ (1003.89): C, 50.25; H, 3.61; N, 2.79; S, 6.39. Found: C, 50.33; H, 3.67; N, 2.74; S, 6.44. HR ESI-MS(+) m/z Cacld. for $[M + 2H]^{2+}$ 502.5747; Found 502.5741. NMR data in $CDCl_3$: δ (^{1}H) 8.07 (s, 2H, H^f), 7.58 (dd, $^3J_{HH}$ = 7.6 Hz, $^3J_{PH}$ = 11.1 Hz, 8H, H°), 7.29 (t, $^3J_{HH}$ = 7.4 Hz, 4H, H^p), 7.19 (t, $^3J_{HH}$ = 7.4 Hz, 8H, H^m), 7.08 (d, $^3J_{HH}$ = 8.3 Hz, 2H, H^d), 6.93 (dd, $^3J_{HH}$ = 8.3 Hz, $^4J_{HH}$ = 2.2 Hz, 2H, H^e), 5.87-5.77 (m, 2H, H^b), 4.98 (d, $^3J_H$$^{c\text{-}cis}$$_H$^{b} = 10.2 Hz, 2H, diastereotopic H^c), 4.81 (d, $^3J_H$$^{c\text{-}trans}$$_H$^{b} = 17.0 Hz, 2H, diastereotopic H^c), 3.39 (m, 4H, H^a); δ (^{19}F{^{1}H}) −61.8 (s, 6F); δ (^{31}P{^{1}H}) 10.1 (s, $^1J_{PtP}$ = 2687 Hz, 2P); δ (^{195}Pt{^{1}H}) −4747.4 (t, $^1J_{PtP}$ = 2686 Hz, 1Pt).

trans-[Pt(PPh$_2$allyl)$_2$(k^1-S-SpyN)$_2$], 1c

Yield: 49 mg, 81%. Elem. Anal. Calcd. for $C_{38}H_{36}N_4P_2PtS_2$ (869.87): C, 52.47; H, 4.17; N, 6.44; S, 7.37. Found: C, 52.32; H, 4.21; N, 6.49; S, 7.41. HR ESI-MS(+) m/z Cacld. for $[M + 2H]^{2+}$ 435.5827; Found 435.5826. NMR data in $CDCl_3$: δ (^{1}H) 7.85 (d, $^3J_{HH}$ = 4.6 Hz, 4H, H^d), 7.74 (dd, $^3J_{HH}$ = 7.9 Hz, $^3J_{PH}$ = 10.6 Hz, 8H, H°), 7.28-7.19 (m, 12H, H^m and H^p), 6.44 (t, $^3J_{HH}$ = 4.6 Hz, 2H, H^f, 6.00-5.91 (m, 2H, H^b), 5.00 (d, $^3J_{H^{c\text{-}cis}H^b}$ = 10.3 Hz, 2H, diastereotopic H^c), 4.88 (d, $^3J_{H^{c\text{-}trans}H^b}$ = 16.4 Hz, 2H, diastereotopic H^c), 3.43 (m, 4H, H^a); δ (^{31}P{^{1}H}) 10.8 (s, $^1J_{PtP}$ = 2766 Hz, 2P); δ (^{195}Pt{^{1}HJ) - 4787.3 (t, $^1J_{PtP}$ = 2771 Hz, 1Pt).

trans-[Pt(PPh$_2$allyl)$_2$(k^1-S-Sbt)$_2$], 1d

Yield: 58 mg, 84%. Elem. Anal. Calcd. for $C_{44}H_{38}N_2P_2PtS_4$ (980.07): C, 53.92; H, 3.91; N, 2.86; S, 13.09. Found: C, 53.98; H, 3.87; N, 2.81; S, 13.16. HR ESI-MS(+) m/z Cacld. for $[M + 2H]^{2+}$ 491.0594; Found 491.0598. NMR data in $CDCl_3$: δ (^{1}H) 7.68 (dd, $^3J_{HH}$ = 8.1 Hz, $^3J_{PH}$ = 9.8 Hz, 8H, H°), 7.55 (d, $^3J_{HH}$ = 8.0 Hz, 2H, H^9), 7.45 (d, $^3J_{HH}$ = 7.9 Hz, 2H, H^d), 7.28-7.16 (m, 14H, H^f, H^m and H^p), 7.11 (t, $^3J_{HH}$ = 7.9 Hz, 2H, H^e), 5.79-5.68 (m, 2H, H^b), 4.93 (d, $^3J_{H^{c\text{-}cis}H^b}$ = 10.2 Hz, 2H, diastereotopic H^c), 4.78 (d, $^3J_{H^{c\text{-}trans}H^b}$ = 16.8 Hz, 2H, diastereotopic H^c), 3.47 (m, 4H, H^a); δ (^{31}P{^{1}H}) 10.9 (s, $^1J_{PtP}$ = 2591 Hz, 2P); δ (^{195}Pt{^{1}H}) −4641.4 (t, $^1J_{PtP}$ = 2589 Hz, 1Pt).

trans-[Pt(PPh$_2$allyl)$_2$(k^1-S-Sbi)$_2$], 1e

Yield: 46 mg, 69%. Elem. Anal. Calcd. for $C_{44}H_{40}N_4P_2PtS_2$ (945.97): C, 55.87; H, 4.26; N, 5.92; S, 6.78. Found: C, 55.98; H, 4.31; N, 5.87; S, 6.72. HR ESI-MS(+) m/z Cacld. for $[M + 2H]^{2+}$ 473.5983; Found 473.5966. NMR data in $CDCl_3$: δ (^{1}H) 10.32 (brs, 2H, NH), 7.45

(dd, $^{3}J_{HH}$ = 7.7, $^{3}J_{PH}$ = 9.6 Hz, 8H, H°), 7.24 (d, $^{3}J_{HH}$ = 7.8 Hz, 2H, H^{g}), 7.21 (d, $^{3}J_{HH}$ = 7.6 Hz, 2H, H^{d}), 7.18-7.04 (m, 12H, H^{m} and H^{p}), 7.01-6.87 (m, 4H, H^{e} and H^{f}), 5.74-5.63 (m, 2H, H^{b}), 4.97 (d, $^{3}J_{H^{c}\text{-}cis_{H^{b}}}$ = 10.0 Hz, 2H, diastereotopic H^{c}), 4.79 (d, $^{3}J_{H^{c}\text{-}trans_{H^{b}}}$ = 16.2 Hz, 2H, diastereotopic H^{c}), 3.48 (m, 4H, H^{a}); δ ($^{31}P\{^{1}H\}$) 10.6 (s, $^{1}J_{PtP}$ = 2643 Hz, 2P); δ ($^{195}Pt\{^{1}H\}$) −4684.8 (t, $^{1}J_{PtP}$ = 2651 Hz, 1Pt).

Single-Crystal Structure Determination

Intensity data for these compounds were collected using a D8 Quest *k*-geometry diffractometer with a Bruker Photon II ccd area detector19 and an Incoatec Iμs microfocus Mo Kα source (λ = 0.71073 Å). The data was corrected for absorption by the empirical method. 20 The crystal system and the space group were determined by systematic absences and statistical tests and verified by subsequent refinement. The structure was solved by direct methods and refined by full-matrix least-squares methods on *F*2.[20] The positions of hydrogens were initially determined by geometry and were refined using a riding model. Non-hydrogen atoms were refined with anisotropic displacement parameters. Hydrogen atom displacement parameters were set to 1.2 times the isotropic equivalent displacement parameters of the bonded atoms.

The molecules in the structure of **1a** are located on the inversion centers; thus, one half of the atoms in the two molecules are unique. The selected crystal for complex **1b** was slightly split (~ 4°), requiring that the intensity data be processed as if the sample were a twin. The molecule was found to sit on a center of symmetry; thus, only one half of the atoms were unique. Also, the metal complex **1c** was located on an inversion center; thus, one half of the atoms are unique. The solvent molecule was in a general position. The CH_2Cl_2 solvent molecule was disordered. The

occupancies of the CH_2Cl_2 refined to 0.73(3) and 0.27(3) for the S and T orientations, respectively. Restraints on the positional and displacement parameters of the solvent were required.

Computational Details

Density functional calculations were performed with the program suite Guassian09[22] using the B3LYP level of theory.[23] The LANL2DZ basis set was chosen to describe Pt[24] and the 6-31G(d) basis set was chosen for other atoms. The geometries of complexes were fully optimized by employing the density functional theory without imposing any symmetry constraints. In order to ensure the optimized geometries, frequency calculations were performed employing analytical second derivatives. Solvent effects have been considered by the conductor-like polarizable continuum model (CPCM).[25]

The crystal structure of **1c** was directly or indirectly employed in order to make input files for the software. The ground state (S0) of **1c** and **1c"** were optimized in gas phase or CH_2Cl_2 solvent and their optimized coordinates were collected.

Biological Assay

Cell lines and cell culture

Human cancer cell lines, MCF-7 (breast cancer), SKOV3 (ovarian cancer), and A549 (non-small cell lung cancer) were purchased from the National Cell Bank of Iran (NCBI, Pasteur Institute, Tehran, Iran). The cells were grown in complete culture media containing RPMI 1640 (Biosera, France), 10% fetal bovine serum (FBS; Gibco, USA), and 1% penicillin-streptomycin (Biosera, France) and kept at 37 °C in a humidified CO_2 incubator. MCF-10A cells (human breast epithelial cell line) were cultured in DMEM/Ham's F-12 (GIBCO-Invitrogen, Carlsbad, CA)

supplemented with 100 ng/ml cholera toxin, 20 ng/ml epidermal growth factor (EGF), 0.01 mg/ml insulin, 500 ng/ml hydrocortisone, and 5% chelex-treated horse serum.

Cytotoxic activities of *trans*-Pt(II) compounds were investigated using a standard 3-(4,5-dimethylthiazol-yl)-2,5-diphenyl-tetrazolium bromide (MTT) assay, as previously described.[4] To do this, the cells with a density of 0.8×10^4 cells per well were seeded in 96-well microplates and kept for 24h to recover. The cells were then treated with compounds series **A** and **1a-e** in different concentrations ranging from 1 to 100 μM in a triplicate manner and incubated for at least 72 hours at 37 °C in humidified CO_2 incubator. Following incubation, the media was completely discarded and replaced with 150 μl of RPMI 1640 containing 0.5 mg/mL MTT solution and incubated at room temperature for 3h. To dissolve the formazan crystals, the media containing MTT was discarded again and 150 μl of DMSO was added to each well and incubated for at least 30 min at 37 °C in the dark. The absorbance of individual well was then read at 490 nm with an ELISA reader. The 50% inhibitory concentration of each compound, representing IC_{50}, was calculated with CurveExpert 1.4. Data are presented as mean ± SD.

Apoptosis assay

BioLegend's PE Annexin V Apoptosis Detection Kit with 7AAD (Biolegend, USA) was used to assess the apoptotic effect of **1a** compound as previously described.[4e] Briefly, 0.5 x 10^5 cells per 1 ml of complete culture medium were seeded in a 24-well culture plate, treated with **1a** compound in different concentrations (2.5, 5 and 10 μM) for 72 h. An untreated sample was also included as a negative control. Treated and untreated cells were then harvested and washed twice with cold BioLegend's Cell Staining Buffer, transferred to the polystyrene round-bottom tubes (BD Bioscience, USA) and stained with 2 μl of PE-conjugated Annexin V and 2 μl

of 7-AAD solution for 15 min at room temperature in the dark. 300 µl of Binding Buffer was added to each tube and analyzed immediately by four-color FACSCalibur flow cytometer (BD Bioscience, USA) with proper setting. The data were analyzed by FlowJo software packages.

Cell cycle analysis

The MCF-7 cells in a total number of 50×10^3 were seeded in a 24-well cell culture plate and treated with two different concentrations of **1a** (1.5 and 2.5 µM). Following 72 hours of incubation, the cells were harvested and washed in PBS 1x. The cells were then fixed in cold 70% ethanol with overnight incubation at 4°C. The fixed cells were washed two times in PBS 1x and centrifuged at 850 ×g. Afterwards, the cells were treated with 50 µl ribonuclease A (100 µg/ml) to ensure only DNA, not RNA, is stained. At the end, 200 µl Propidium Iodide (PI, 50 µg/ml) solution were added to stain DNA. The cells were finally acquired on four-color FACSCalibur flow cytometer (BD Bioscience, USA) with proper setting and analyzed by FlowJo software.

Shift mobility assay

The shift mobility assay was applied to assess the direct interaction of **1a** with DNA. For this purpose, as previously described,[6] the same aliquots of circular form of pGEM-FT plasmid was diluted in a buffer containing Tris-HCl (pH=8.5) in the presence of different concentrations of **1a** (100, 200 and 400 µm) and then incubated at 37 °C for 24h. Cisplatin in the same concentrations as well as untreated DNA were also included as positive and negative controls, respectively. Afterward, 10 µl of each sample were mixed with 5 µl KBC loading dye (Kawsar

Biotec, Iran) and electrophoresed for 3 hours at 70 V in 0.5% TEA buffer in 1 % agarose gel (Invitrogen, USA) and then visualized by a UV detector.

Comet assay

We also assessed the genotoxic ability of **1a** compound using comet assay. To do this, 5 × 10^5 MCF7 cells in 2 ml complete culture medium were prepared and treated with two different concentrations of **1a** (10 and 50 μM). Untreated as well as Doxorubicin treated (1 μM) cells were also included as negative and positive controls, respectively. The cells were incubated for 20 min at 37°C in a humidified incubator with 5% CO2. The cells were then participated, re-suspended in 100 μl 1× PBS, mixed with low melting point agarose (LMPA) and dropped on a slide pre-coated slide with normal melting point agarose (NMPA) layer. A coverslip was placed over the gel and set at 4°C for 15 min. The coverslip was then removed and 100 μl of LMPA was added onto the agarose gel mixture layer, covered with a new coverslip, and placed at 4°C for 15 min. The coverslip was then removed, and the slides were immersed into cold lysis solution and refrigerated overnight and then in fresh cold alkaline electrophoresis buffer for 40 min. The slides were electrophoresed with the adjusted voltage (24 V) and current (300 mA). Afterward, the slides were flooded with neutralizing Tris buffer (pH=7.4) and distilled water for 5 min, and then in 70%, 90% and 100% Ethanol (Merck, Germany) sequentially. The slides were lastly stained with 100 μl PI (50μg/ml) and visualized by a high resolution fluorescent microscopy (BX61, Olympus). The images were taken at 20× magnification and analyzed by the Olympus micro imaging software CellSens (Olympus, Japan).

Determination of Intracellular Reactive Oxygen Species (ROS)

Cellular Reactive Oxygen Species Detection Assay Kit (TEB PAZHOUHAN RAZI, Iran) was used to determine the oxidative stress response in SKOV3 cell lines following treatment with **1a** according to manufacture instruction with a little modification. Briefly, SKOV3 cells were grown in complete culture media, harvested as a single cell suspension with a density of 300×10^3 and treated with 10, 20 and 40 μM for 2 h at 37°C. Untreated cells were also included as negative control. After incubation, the cells were washed two times with buffer R1 and stained with R2 buffer containing 2',7'-Dichlorodihydrofluorescein diacetate (DCFH-DA) prepared in phenol red negative RPMI culture media (Biosera, France) for 1 h at 37°C. The H_2O_2 (1000 μM) were added to the control positive tube and incubated for more 20 min. The cells were then washed with R1 buffer and subjected to flow cytometry analysis immediately. At least 15000 events were acquired on four color FACSCalibur flow cytometer (BD Biosciences, USA) and analyzed by FlowJo software v10.

Results and Discussion

Synthesis and characterization

Figure 2 clearly demonstrates the general synthetic route for the new complexes. The starting complex *cis*-[Pt(PPh_2allyl)$_2Cl_2$], **A**, was synthesized through ligand exchange, by the reaction of allydiphenylphosphane (PPh_2allyl) with known complex *cis,trans*-[$PtCl_2(SMe_2)_2$][17] or *cis*-[$PtCl_2$(dmso)$_2$][18]. The dimethyl sulfide (SMe_2) and dimethyl sulfoxide (dmso) displace with monodentate phosphane ligand under mild conditions. Treatment of **A** (in CH_2Cl_2) with ethanolic solution of potassium thionate salts (KSR) produced new platinum(II) complexes of general

formula *trans*-[Pt(PPh$_2$allyl)$_2$(k^1-S-SR)$_2$], SR = deprotonated form of pyridine-2-thiol (Spy, **1a**), 5-(trifluoromethyl)-pyridine-2-thiol (SpyCF$_3$-5, **1b**), pyrimidine-2-thiol (SpyN, **1c**), benzothiazole-2-thiol (Sbt, **1d**) and benzimidazole-2-thiol (Sbi, **1e**).

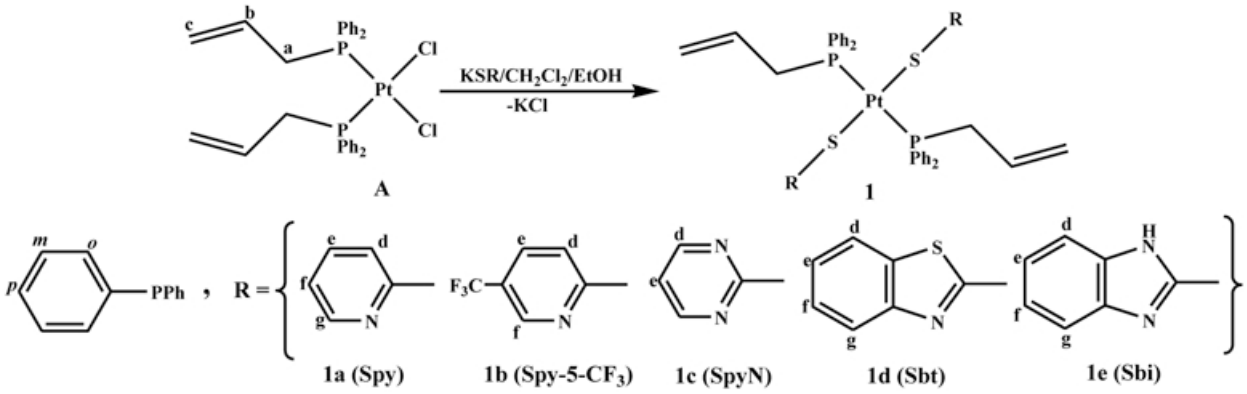

Figure 2. *Preparation of trans-Pt(II) complexes with heterocyclic thionate ligand.*

The *cis-trans* isomerization (from **A** to **1a-e**) was previously detected in some Pt(II) complexes during the chloride ligand replacement with bulky thiolate ligands. However, density functional theory (DFT) was used to support this observation and get more insight into this isomerization. DFT was applied by the optimization of the lowest energy structures, either gas phase or CH_2Cl_2 solution, of the proposed *cis* and *trans* geometries for **1c** as a case study in this calculation, which is shown in Figure 3.

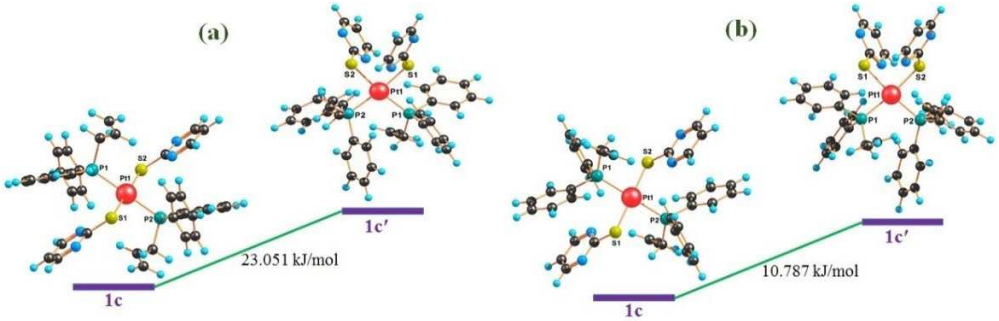

Figure 3. *The energy difference between* ***1c*** *and its corresponding cis isomer* ***1c'*** *in (a) gas phase and (b) CH_2Cl_2 solution.*

The DFT calculation indicated that the *trans* isomer **1c** is much more stable than the suggested *cis* isomer **1c'** in both states. In gas phase, **1c** is more stable than **1c'** by 23.051 kJ/mol. In the CH_2Cl_2 solution, the difference between **1c** and **1c'** is equal to 10.787 kJ/mol (Figure 3). Additionally, the NMR spectra and X-ray crystallography supported that the theoretical calculations correctly predicted the preferred *trans* configuration.

The formulae proposed for **A** and **1a-e** were confirmed by HR ESI-Mass analysis. The ESI-Mass spectra of these complexes were recorded in the positive mode and in a dilute acetonitrile solution. The HR ESI-Mass(+) spectrum for **A** displayed the presence of molecular ion $[M - 2CI]^{2+}$, whereas the HR ESI-Mass(+) spectra for **1a-e** revealed the molecular ion $[M + 2H]^{2+}$ as the most intense peak in the complexes. The NMR labeling of ligand moieties are depicted in Figure 2, for clarifying the chemical shift assignments. The main resonances of functional groups for phosphane ligand in **A** are derived from ^{1}H NMR spectroscopy. The $^{31}P\{^{1}H\}$ NMR spectrum of **A** has revealed one singlet resonance at δ = 4.6 ppm flanked by Pt satellites ($^{1}J_{PtP}$= 3671 Hz) which is attributed to the PPh_2allyl moieties in *cis*-dipositions. This signal has been cleanly shifted to the lower fields in *trans*-configured Pt(II) complexes accompanied by decreasing in the coupling constant between platinum atom and phosphorus atom, for instance, in the case of complex **1c,** δ = 10.8 ppm ($^{1}J_{PtP}$= 2766 Hz). The $^{1}J_{PtP}$ value is indicative of the electron-donating character of the *cis*- or *trans*-positioned ligands. The lowering of this value is good evidence to rule out the formation of the *cis* configuration in the thiolate complexes and is consistent with a *trans* feature (**1a-e**). Confirming earlier observations in the $^{31}P\{^{1}H\}$ NMR spectra by the $^{195}Pt\{^{1}H\}$ NMR spectra of complexes **A** and **1c** (selected as case study) demonstrated a triplet resonance at δ = −4420.1 ppm with $^{1}J_{PtP}$ value of 3679 Hz and δ = −4787.3 ppm with $^{1}J_{PtP}$ = 2771 Hz, respectively, corresponding to the coupling among Pt(II) center and PPh_2allyl ligand. In the ^{1}H

NMR spectra of **1a-e,** all the characteristic resonances of PPh_2allyl ligands as well as S-coordinated thionate moieties have been clearly distinguished. The colorless (**A** and **1c**) or yellow (**1a** and **1b**) single crystals, suitable for X-ray diffraction, were obtained by slow diffusion of *n*-hexane into a CH_2Cl_2 solution of each product at room temperature. An ORTEP representation of **A** and **1a-c** are determined in Figure 4. **A** crystallized in the monoclinic (space group *P*21/n), while **1a-c** crystallized in the triclinic (space group *P* 1–) crystal systems. The molecular structure of precursor **A** evidently shows two PPh_2allyl ligands in a *cis* configuration while the molecular structures of **1a-c** display two PPh_2allyl ligands in a *trans* position. Two allydiphenylphosphanes (P1, P2) and two chloride ligands (Cl1, Cl2) in **A** or two PPh_2allyl (P1, P#1) and two sulfur atoms (S1, S#1) in **1a-c** entirely surrounded the Pt(II) center (Figure 4). The geometry around the platinum center in **A** and **1a-c** is considered a slightly distorted square-planar. The angle subtended by the phosphane ligands at the Pt(II) center in **A** (P1-R1-P2 = 99.65(8)°), deviates from the 90° indicative of a distorted planar environment. The angles of P1-Pt1-P P#1 and S1-Pt1-S#1 in **1a-c** are 180.0° but other angles between thiolates and phosphane ligands are deviated from the 90°. As depicted by perspective ORTEP view of the structures (Figure 4), the allyl substituents of the PPh_2allyl phosphane ligands are obviously detected to be perpendicular to the molecule plane in each structure. The distances between Pt(II) and the PPh_2allyl moieties (Pt1-P1 = 2.241(2) Å and Pt1-P2= 2.238(3) Å) in **A,** (Pt1A-P1A = 2.2980(4) Å and Pt1 B-P1B 2.3129(4) Å) in **1a,** or (Pt1-P1 = 2.3015(6) Å) in **1b** and (Pt1-P1 = 2.3031(5) Å) in **1c,** are in the same range as those found in similar Pt(II)-phosphane complexes. The distances of the Pt–S bonds are almost equal in **1a-c** (~2.33 Å). It is notable that the pyridyl moiety in the k^1-S-SR ligand is approximately perpendicular to the metal plane.

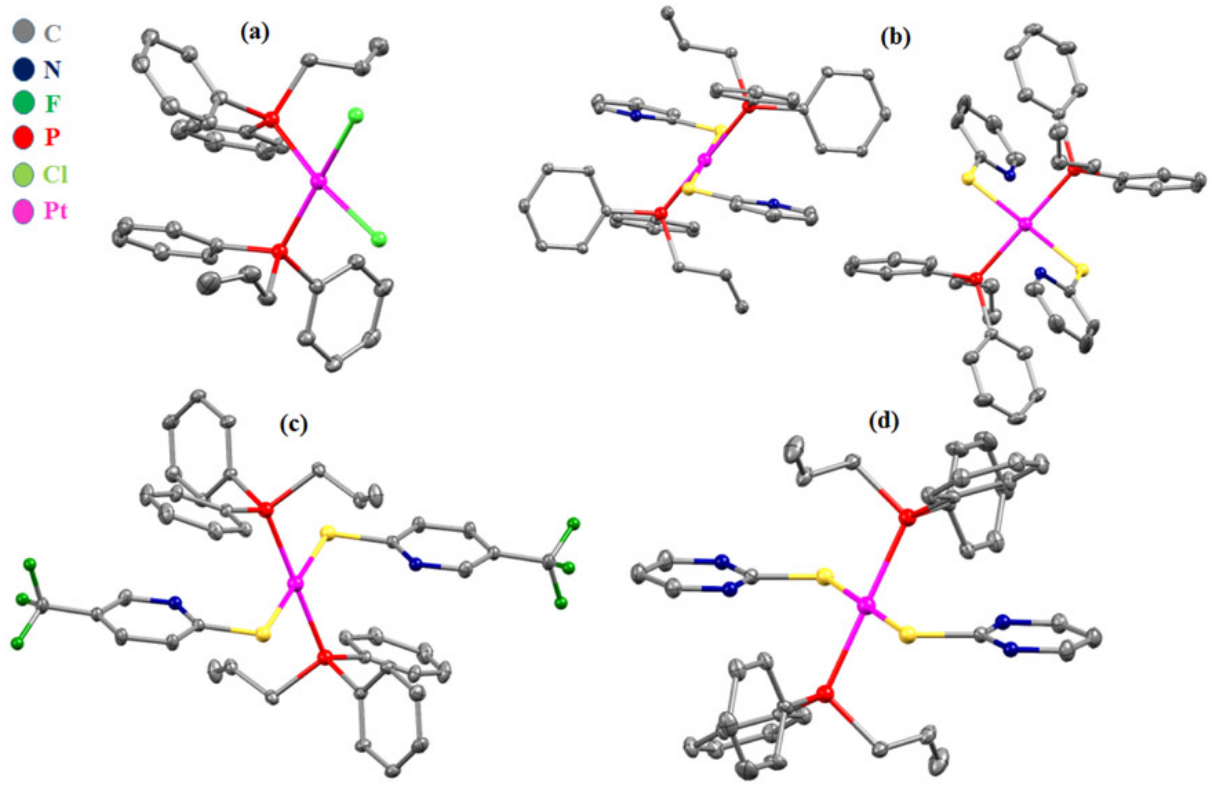

Figure 4. ORTEP plot molecular structures of **A** and **1 a-c** drawn at 50 % probability level. Selected bond lengths (Å) and angles (deg) for complexes: (a) **A**: Pt1-**35** Cl1 2.352(2), Pt1-Cl2 2.346(3), Pt1-P1 2.241(2), Pt1-P2 2.238(3); Cl1-Pt1-Cl2 88.50(9), P1-Pt1-P2 99.65(8), Cl1-Pt1-P1 151.57(8), Cl2-Pt1-P2 168.14(9); (b) **1 a**: Pt1A- P1A 2.2980(4), Pt1B-P1B 2.3129(4), Pt1A-S1A 2.3261(4), Pt1B-S1B 2.3310(4), P1A-Pt1A-P#1 A 180.0, P1B-Pt1B-P#1B 180.0, S1A-Pt1A-S#1 A 180.0, S1B-Pt1B-S#1B 180.0; (c) **1 b**: Pt1-P1 2.3015(6), Pt1-S1 2.3313(5), P1-Pt1-P#1 180.0, S1-Pt1-S#1 180.0, P1-Pt1-S1 84.840(18), P1-Pt1-S#1 95.160(18); (d) **1 c**: Pt1-P1 2.3031(5), Pt1-S1 2.3328(5), P1-Pt1-P#1 180.0, S1-Pt1-S#1 180.0, P1-Pt1-S1 94.710(16), P1-Pt1-S#1 85.289(16), P#1-Pt1-S1 85.291(16), P#1-Pt1-S#1 94.710(16). Hydrogen atoms and CH_2Cl_2 solvent molecules (**A** and **1 c**) were omitted for clarity.

Biological activity studies

The *in vitro* cytotoxic activity of **A** and **1a-e** were evaluated on three cancer cell lines including human lung (A549), ovarian (SKOV3), and breast (MCF-7) carcinoma. As shown in Table 1, **1a,** showed higher anti-proliferative activity than cisplatin on the studied cell lines. It showed a good anti-proliferative activity with IC_{50} of 4.31, 6.23 and 4.80 μM comparing with those measured for cisplatin (9.71, 14.48 μM and 11.59 μM, against A549, SKOV3 and MCF-7 cell lines, respectively). One-way ANOVA statistical analysis showed that the differences between

1a and cisplatin is statistically significant. **1b** also displayed better *in vitro* cytotoxicity than cisplatin on SKOV3 cell line with IC_{50} of 12.38 μM, however this difference is not statistically significant. **1b** and cisplatin IC_{50} on A549 cell line was also not statistically significant. **1c** and cisplatin IC_{50} on SKOV3 cells was also not statistically significant. Complexes **A, 1b, 1c,** and **1e** also showed antitumor activity against MCF-7 cell line in comparison with cisplatin. It should be mentioned that the cytotoxicity of all the ligands including Spy, Spy-5-CF_3, SpyN, Sbt, Sbi and allydiphenylphosphane (PPh_2allyl) was evaluated against A549 cell line and the IC50 of all the ligands was more than 100 μM.

Complex	**(IC_{50} ± SD) μM**			
	A549	**SKOV3**	**MCF-7**	**MCF-10A**
A	22.49 ± 1.62	34.50 ± 1.53	19.01 ± 1.24	68.74 ± 1.21
1a	4.31 ±0.72	6.23 ± 0.74	4.80 ± 0.71	38.42 ± 2.06
1b	12.59 ± 1.09	17.49 ± 1.21	19.68± 1.59	53.26 ± 1.13
1c	16.01 ± 1.12	12.38 ± 1.17	15.64 ± 1.37	44.71 ±1.42
1d	20.15 ± 1.47	22.14 ± 1.67	34.65 ± 0.83	88.42 ±1.39
1e	18.62 ± 1.55	21.73 ± 1.19	17.45 ± 1.71	47.06 ± 0.83
Cisplatin	9.71 ± 1.70	14.48 ± 1.54	11.59 ± 1.66	29.47 ± 1.03

Table 1. *In vitro cytotoxicity of all the synthesized compounds against cancerous and non-cancerous cell lines*

Furthermore, to verify the selectivity between cancer and normal cell lines, the effects of these compounds on the proliferation on non-cancerous cell line (MCF-10A; normal human epithelial breast cell line) were also determined. As shown in Table 1, all these compounds

displayed reasonable selectivity between tumorigenic and non-tumorigenic cell lines and showed less cytotoxicity than cisplatin on MCF-10A cell line. Structure-activity relationship studies revealed that, generally, the complex **A** which includes a chloro group instead of a thionate ligand, showed lower anti-proliferative activity than other. Among thiolated ligands, **1b** with a thiolated pyrimidine ring and especially, **1a** with a thiolated pyridine ring showed the highest potency.

Determining apoptotic effect of 1a on MCF-7 cell line.

BioLegend's PE Annexin V Apoptosis Detection Kit was used with 7AAD to specifically determine the dose-dependent apoptotic effect of complex **1a** on cancerous cells. To determine this, **1a** with three concentrations (2.5, 5, and 10 μM) was applied onto MCF-7 cells. As illustrated in Figure 5, with the increase in the concentration of **1a** from 2.5 to 10 μM, the percentage of the cells in early apoptotic phase significantly increases from 7.8% in untreated cells to 11.0%, 40.8%, and 62.9% in the treated cells. This observation indicates that compound **1a** as a representative of the new *trans*-Pt(II) complexes is able to effectively induce apoptosis in cancerous cells in a dose dependent manner. Also, the observed antiproliferative/cytotoxic effect for **1a** in cytotoxic assay could be partly mediated through inducing apoptosis in cancer cells.

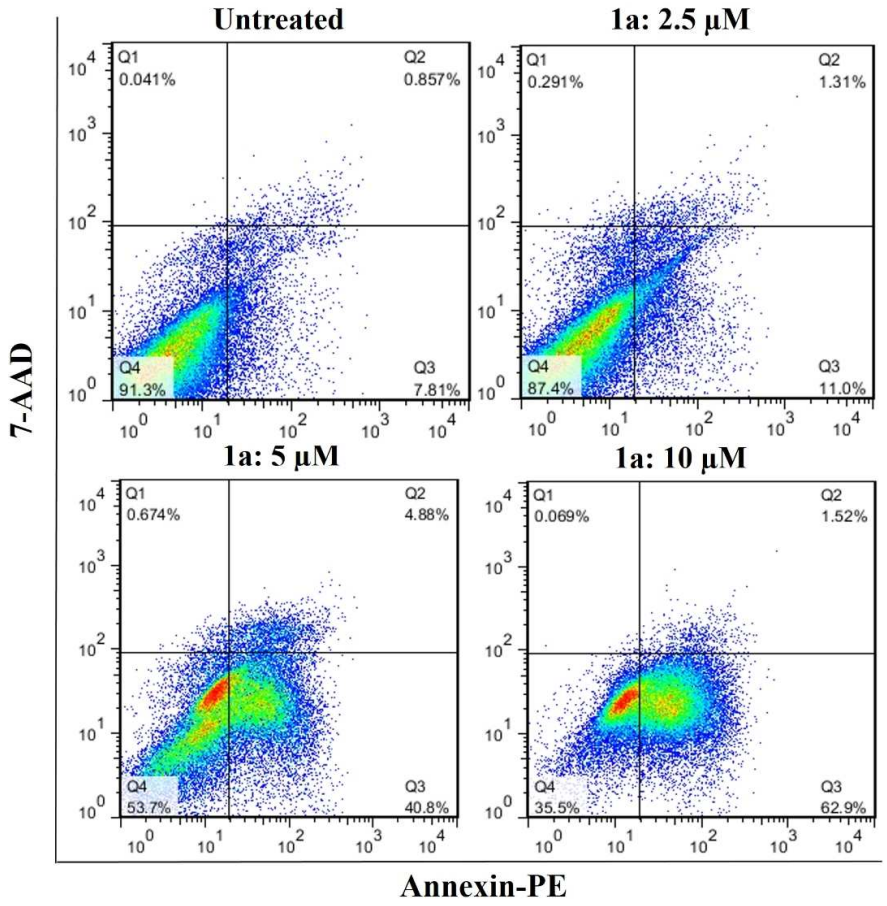

Figure 5. *Flow cytometric analysis of apoptotic effect of **1a.** MCF-7 cells (Human breast carcinoma) were left untreated (A) or treated for 48 h with 2.5, 5, and 10* µM *of **1a.** Q1: necrotic cells, Q2: late apoptotic cells, Q3: early apoptotic cells, and Q4: living cells.*

The potential effect of 1a on MCF-7 cells' cell cycle

Quantitation of DNA content using flow cytometry or cell cycle analysis is a basic method which is commonly used to assess the mechanisms of antiproliferative effects of anticancer drugs. In this method, a fluorescent DNA binding dye (in this study: propidium iodide, PI) is used to stain DNA and measure the amount of DNA present in the cell. The cells in the G2 phase are expected to absorb approximately twice the amount of color compared to the cells in G1 as their DNA content has been doubled during S phase. Therefore, the cells in S phase have more DNA than G1 cells but less than G2 ones. Therefore, we were able to check whether our compound exerts its antitumor effects thorough modifying cell cycle or not. As observed in Figure 6, comparing to

untreated cells, no obvious change in different cycle phases could be observed which probably shows that 1a has no clear effect on the cell cycle of cancerous cells.

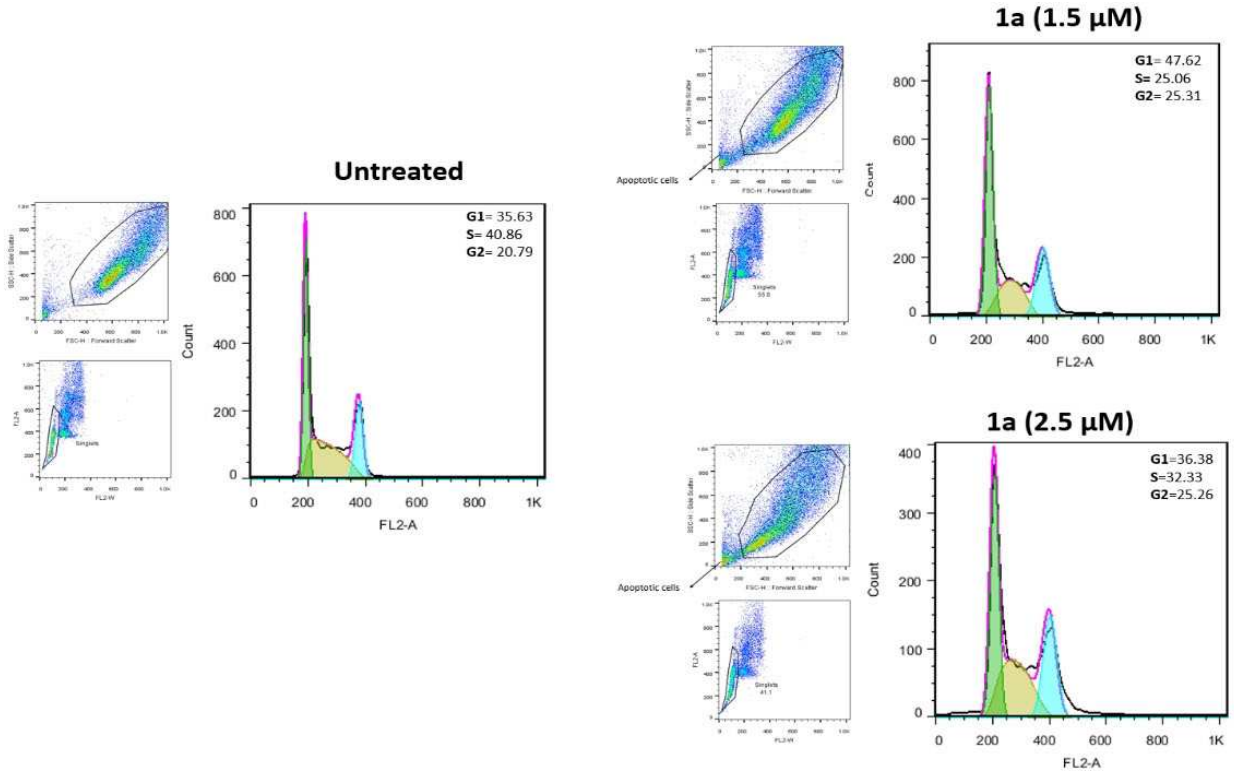

Figure 6. *The effect of **1a** on the cell cycle in MCF-7 cells.*

Genotoxicity and DNA interaction

Comet assay was used as a valuable method to predict the genotoxic effect of new synthesized *trans*-Pt(II) complexes on cancerous cells. In this single cell microgel electrophoresis method, following the DNA damage, the migration of chromosomal DNA from the nucleus increases and resembles the shape of a tail or comet. The longer tails display the more genotoxicity, whilst untreated cells as un-fragmented cells, represent a little or no tail. In the current study, we checked the genotoxicity of **1a** as the best cytotoxic compound in the **1** series through comet assay. As could be observed Figure 7, treatment of MCF-7 cells with both low and high concentrations

of **1a** (10 and 50μM), results in the appearance a relatively long tail following the electrophoresed cells in the concentration of 10 μM, which shows strong genotoxic ability of **1a**. In the case of a concentration of 50, as displayed in Figure 7D, no nucleus remained and only a blurry tail of degraded DNA could be seen. These observations collectively showed that **1a** compound intensely targets the genome content of cancerous cells. However, in electrophoresis mobility shift assay which used to further show the direct interaction of **1a** compound with DNA, a little shift was observed comparing to cisplatin as positive control in Figure 8. It could also be seen that compared to the untreated control, **1a** could make a nick in DNA and subsequently slightly shift the mobility of the plasmid in a dose dependent manner. These observations confirm the direct interaction of **1a** with DNA through genotoxic effect as observed in comet assay. This clearly indicates that the effective mechanisms of these compounds have a direct interaction with DNA and probably other molecules as well. These results are collectively consistent with previous studies which have described platinum compounds as DNA-targeting metal-based anticancer agents.[14]

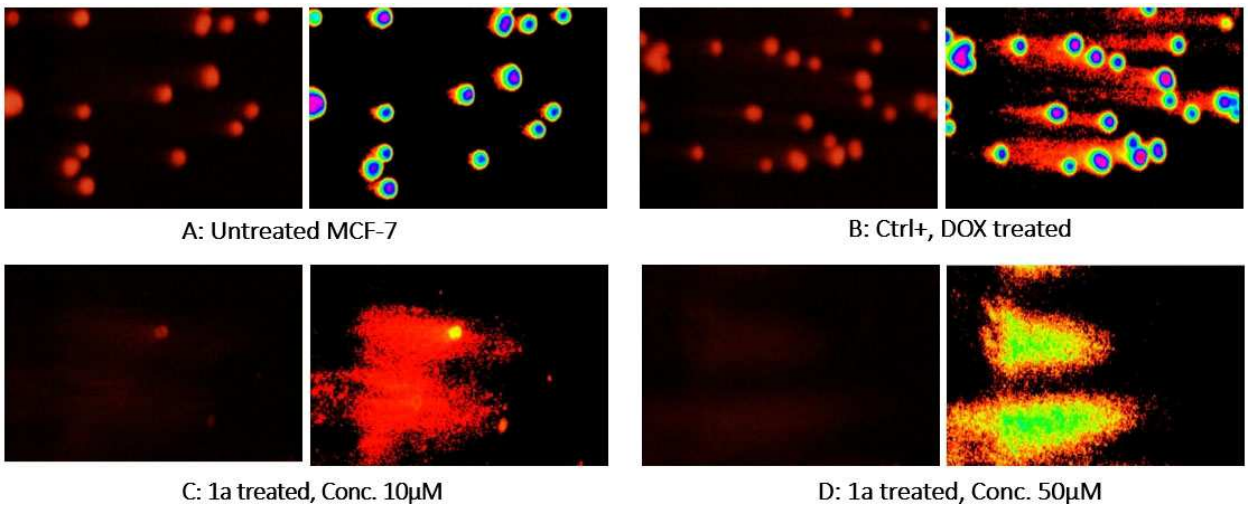

Figure 7. Genotoxic effect of **1a** on MCF-7 cell line. The percentage of degraded DNA in the tail has remarkably increased following treatment with doxorubicin (B: Docorubicin) as a positive control and different concentrations of **1a** (C and D) in comparison to untreated cells (A: negative control). For better resolution, the same pictures from CometScore software are also shown.

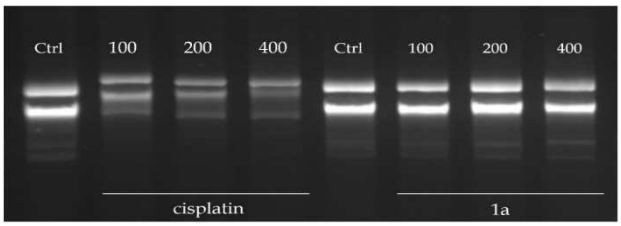

Figure 8. Mobility shift assay of **1a** compound. pGEM-FT plasmid in circular form was incubated with different concentrations of cisplatin (positive controls) as well as compound 1a for 24h.

In order to determine the binding mode and binding site of the *trans*-Pt(II) complexes in interaction with DNA, molecular docking studies was also employed. As shown in Figure 9, **1d** fitted into the minor groove of DNA and interacts through its sulfur groups via weak hydrogen bonding with G4 and C11 base pairs in the minor groove of DNA.

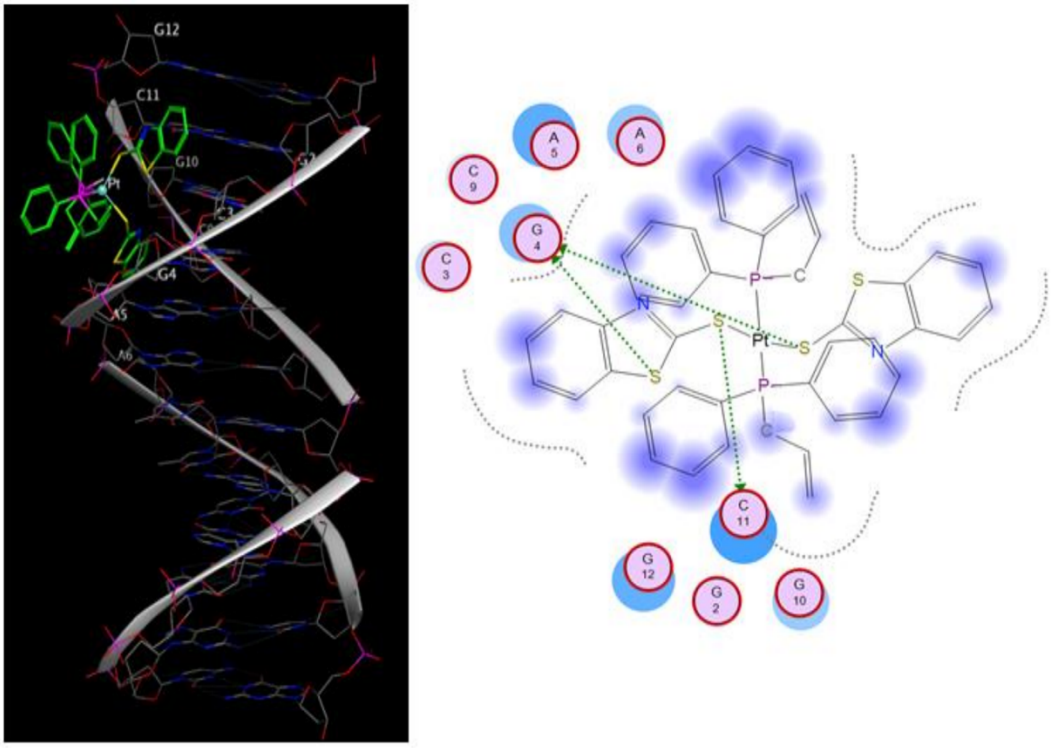

Figure 9. Molecular docking studies of **1d** in binding with DNA (PDB ID: 1BNA)

Intracellular Reactive Oxygen Species (ROS) Determination

A flow cytometry based method was used for determination of cellular reactive oxygen species (ROS) in SKOV3 cell line after treatment with **1a.** In this highly sensitive method, to consider ROS formation, SKOV3 cells were treated with **1a** and H_2O_2 (positive control) and stained with 2',7'-Dichlorodihydrofluorescein diacetate (DCFH-DA), a cell-permanent non-fluorescent dye which is oxidized by cellular ROS and produce 2',7'- dichlorofluorescein (DCF) fluorescent component. The intensity of DCF is a direct estimate of the amount of ROS within the cells. As illustrated in Figure 10, treatment of SKOV3 cells with **1a** moderately induce ROS in a relatively dose dependent manner, however the production of ROS was higher in lower concentration of **1a** (10 μM) comparing to higher concentration (40 μM) (Figure 10).

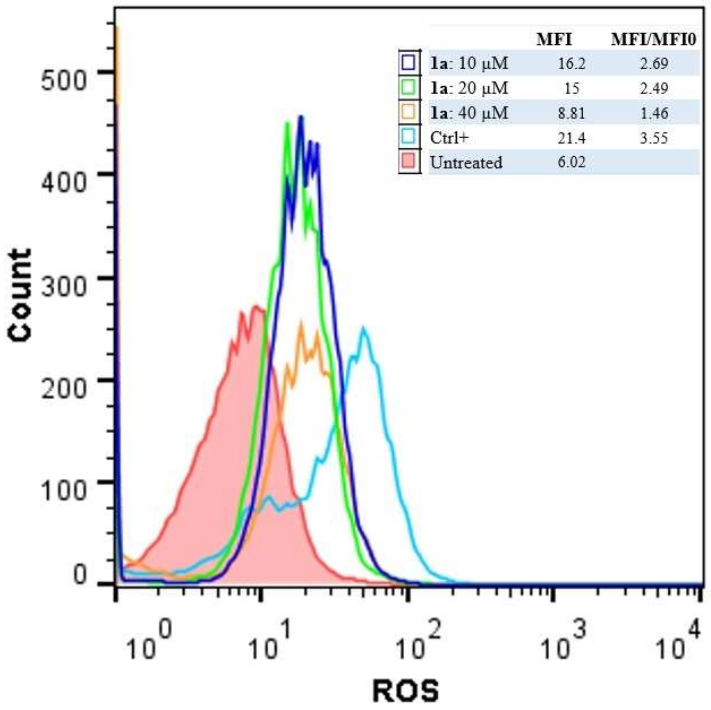

Figure 10. Generation of ROS in SKOV3 cells induced by various concentrations of **1a** and H_2O_2 as positive control. Changes in ROS levels were expressed as a ratio of the mean fluorescence intensity (MFI) in each condition divided by the basal intensity of the ROS at the untreated cells (negative controls, MFI0). H_2O_2 could induce ROS production within 20 minutes (light blue line). Compound **1a** at all concentrations could induce ROS production in SKOV3 cell line. However in lower concentrations, 10 μM (dark-blue line) **1a** is more efficient than higher concentrations, 20 μM (green line) and 40 μM (orange line), in comparison to untreated cells (red filled).

Conclusions and Future Directions

Ultimately, a synthetic approach has been introduced to obtain a class of platinum complexes with the general formula trans-[Pt(PPh_2allyl)$_2$(k^1-S-SR)2], **1**, PPh_2allyl = allyldiphenylphosphine, SR = deprotonated form of pyridine-2-thiol (Spy, **1a**), 5-(trifluoromethyl)-pyridine-2-thiol (SpyCF_3-5, **1b**), pyrimidine-2-thiol (SpyN, **1c**), benzothiazole-2-thiol (Sbt, **1d**) and benzimidazole-2-thiol (Sbi, **1e**). NMR spectroscopy was an important tool to accurately characterize the new Pt(II) complexes. Furthermore, single X-ray crystallography was used to confirm the *cis*-configuration of PPh_2allyl ligands in starting complex **A**. The X-ray crystal structure determined that the heterocyclic thionate ligands are bound to the Pt(II) center with S-coordinating mode with trans-positioned to each other. Also, all newly synthesized Pt(II) complexes were tested against three human cancer cell lines including lung (A549), ovarian (SKOV3) and breast (MCF-7), which showed potent antitumor activities. *In vitro* studies introduced **1a** as a therapeutic agent due to the inhibition growth of MCF-7 cancer cell, mediated through inducing apoptosis. According to the observations, **1a** has the highest affinity to the DNA *in vitro* and considerable potential for additional development as an anticancer agent. Further studies are needed to provide new insights into accurately exploring the mechanism of action of platinum drugs within biological systems, which will lead to the development of new effective anticancer metallodrugs.

By utilizing this new and reliable strategy for the preparation of trans-Pt(II) complexes, resistance to conventional Pt treatment may be overcome. Changing the configuration of Pt(II) complexes and utilizing thionate ligands is an excellent approach to bring cytotoxic effects and bioactivity to cancerous cells. These new Pt(II) drugs have great potential in the area of anticancer therapy and treatment.

References

1. Siegel, R. L.; Miller, K. D.; Jemal, A., Cancer statistics, 2019. *CA Cancer J. Clin.* **2019**, *69*, 7-34.
2. Kenny, R. G.; Marmion, C. J., Toward Multi-Targeted Platinum and Ruthenium Drugs: A New Paradigm in Cancer Drug Treatment Regimens? *Chem. Rev.* **2019**, *119*, 1058-1137.
3. a) F. M. Muggia, A. Bonetti, J. D. Hoeschele, M. Rozencweig, S. B. Howell, [25] **55** *J. Clin. Oncol.* **2015**, *33*, 4219–4226; b) F. Arnesano, G. Natile, *Coord.Chem. Rev.* **2009**, *253*, 2070–2081; c) Y. Jung, S. J. Lippard, *Chem. Rev.* **2007**, *107*, 1387–1407.
4. a) E. Lalinde, R. Lara, I. P. López, M. T. Moreno, E. Alfaro-Arnedo, J. G. Pichel, S. Piñeiro-Hermida, *Chem. Eur. J.* **2018**, *24*, 2440–2456; b) M. V. Babak, M. Pfaffeneder-Kmen, S. M. Meier-Menches, M. S. Legina, S. Theiner, C. Licona, C. Orvain, M. Hejl, M. Hanif, M. A. Jakupec, B. K. Keppler, C. Gaiddon, C. G. Hartinger, *Inorg. Chem.* **2018**, *57*, 2851–2864; c) M. Frezza, Q. P. Dou, Y. Xiao, H. Samouei, M. Rashidi, F. Samari, B. Hemmateenejad, *J. Med. Chem.* **2011**, *54*, 6166–6176; d) F. Samari, B. Hemmateenejad, M. Shamsipur, M. Rashidi, H. Samouei, *Inorg. Chem.* **2012**, *51*, 3454–3464; e) M. Fereidoonnezhad, H. R. Shahsavari, S. Abedanzadeh, B. Behchenari, M. Hossein-Abadi, Z. Faghih, M. H. Beyzavi, *New J. Chem.* **2018**, *42*, 2385–2392.
5. S. Ahmad, *Chem. Biodiversity* **2010**, *7*, 543–566.
6. J. Reedijk, *Eur. J. Inorg. Chem.* **2009**, *2009*, 1303–1312.
7. S. Ahmad, *Polyhedron* **2017**, *138*, 109–124.
8. a) N. Farrell, T. T. Ha, J. P. Souchard, F. L. Wimmer, S. Cros, N. P. Johnson, *J. Med. Chem.* **1989**, *32*, 2240–2241; b) L. R. Kelland, C. F. Barnard, K. J. Mellish, M. Jones, P. M. Goddard, M. Valenti, A. Bryant, B. A. Murrer, K. R. Harrap, *Cancer Res.* **1994**, *54*, 5618–5622; c) N. Farrell, L. R. Kelland, J. D. Roberts, M. Van Beusichem, *Cancer Res.* **1992**, *52*, 5065–5072; d) S. Miranda, E. Vergara, F. Mohr, D. de Vos, E. Cerrada, A. Mendía, M. Laguna, *Inorg. Chem.* **2008**, *47*, 5641–5648; e) E. Guerrero, S. Miranda, S. Lüttenberg, N. Fröhlich, J.-M. Koenen, F. Mohr, E. Cerrada, M. Laguna, A. Mendía, *Inorg. Chem.* **2013**, *52*, 6635–6647; f) E. Vergara, S. Miranda, F. Mohr, E. Cerrada, E. R. T. Tiekink, P. Romero, A. Mendía, M. Laguna, *Eur. J. Inorg. Chem.* **2007**, *2007*, 2926–2933.
9. S. Sieste, I. Lifincev, N. Stein, G. Wagner, *Dalton Trans.* **2017**, *46*, 12226– 12238.
10. N. Farrell, *Met. Ions Biol. Syst.* **1996**, *32*, 603–639.
11. a) R. C. Todd, S. J. Lippard, *Metallomics* **2009**, *1*, 280–291; b) N. J. Wheate, S. Walker, G. E. Craig, R. Oun, *Dalton Trans.* **2010**, *39*, 8113–8127.
12. S. A. Abramkin, U. Jungwirth, S. M. Valiahdi, C. Dworak, L. Habala, K. Meelich, W. Berger, M. A. Jakupec, C. G. Hartinger, A. A. Nazarov, *J. Med. Chem.* **2010**, *53*, 7356–7364.
13. a) K. Akdi, R. A. Vilaplana, S. Kamah, J. A. Navarro, J. M. Salas, F. Gonzalez-Vılchez, *J. Inorg. Biochem.* **2002**, *90*, 51–60; b) F. Gumus, G. k. e. Eren, L. Açık, A. Celebi, F. Ozturk, S. u. k. Yılmaz, R. I. Sagkan, S. Gur, A. Ozkul, A. Elmalı, *J. Med. Chem.* **2009**, *52*, 1345–1357.
14. M. Fereidoonnezhad, H. R. Shahsavari, E. Lotfi, M. Babaghasabha, M. Fakhri, Z. Faghih, Z. Faghih, M. H. Beyzavi, *Appl. Organomet. Chem.* **2018**, *32*, e4200.
15. a) S. S. Gunatilleke, C. A. F. De Oliveira, J. A. McCammon, A. M. Barrios, *J. Biol. Inorg. Chem.* **2008**, *13*, 555–561; b) S. Urig, K. Fritz-Wolf, R. Réau, C. Herold-Mende, K. Tóth, E. Davioud-Charvet, K. Becker, *Angew. Chem. Int. Ed.* **2006**, *45*, 1881–1886; *Angew. Chem.* **2006**, *118*, 1915–1920.
16. B. S. Furniss, *Vogel's textbook of practical organic chemistry*, Pearson Education India, **1989**.

17. G. S. Hill, M. J. Irwin, C. J. Levy, L. M. Rendina, R. J. Puddephatt, R. A. Andersen, L. Mclean, *Inorg. Synth.* **1998**, *32*, 149–153.
18. R. Melanson, F. D. Rochon, *Can. J. Chem.* **1975**, *53*, 2371–2374.
19. a) E. Prince, International Tables for X-ray Crystallography, Vol C, Kluwer Academic Publisher, Doordrecht, The Netherlands, **1995**; b) G. M. Sheldrick, SHELX97. Program for Crystal Structure Refinement. Univer- sity of Göttingen, Germany, **1997**.
20. L. Krause, R. Herbst-Irmer, G. M. Sheldrick, D. Stalke, *J. Appl. Crystallogr.* **2015**, *48*, 3-10.
21. a) G. Sheldrick, *Acta Crystallogr.* **2015**, *A71*, 3–8; b) G. Sheldrick, *Acta Crystallogr.* **2015**, *C71*, 3–8.
22. M. J. Frisch, G. W. Trucks, H. B. Schlegel, G. E. Scuseria, M. A. Robb, J. R. Cheeseman, G. Scalmani, V. Barone, B. Mennucci, G. A. Petersson, H. Nakatsuji, M. Caricato, X. Li, H. P. Hratchian, A. F. Izmaylov, J. Bloino, G. Zheng, J. L. Sonnenberg, M. Hada, M. Ehara, K. Toyota, R. Fukuda, J. Hasegawa, M. Ishida, T. Nakajima, Y. Honda, O. Kitao, H. Nakai, T. Vreven, J. J. A. Montgomery, J. E. Peralta, F. Ogliaro, M. Bearpark, J. J. Heyd, E. Brothers, K. N. Kudin, V. N. Staroverov, T. Keith, R. Kobayashi, J. Normand, K. Raghavachari, A. Rendell, J. C. Burant, S. S. Iyengar, J. Tomasi, M. Cossi, N. Rega, J. M. Millam, M. Klene, J. E. Knox, J. B. Cross, V. Bakken, C. Adamo, J. Jaramillo, R. Gomperts, R. E. Stratmann, O. Yazyev, A. J. Austin, R. Cammi, C. Pomelli, J. W. Ochterski, R. L. Martin, K. Morokuma, V. G. Zakrzewski, G. A. Voth, P. Salvador, J. J. Dannenberg, S. Dapprich, A. D. Daniels, O. Farkas, J. B. Foresman, J. V. Ortiz, J. Cioslowski, D. J. Fox, *Gaussian 09, Revision B.01*, **2010**.
23. a) A. D. Becke, *J. Chem. Phys.* **1993**, *98*, 5648–5652; b) B. Miehlich, A. Savin, H. Stoll, H. Preuss, *Chem. Phys. Lett.* **1989**, *157*, 200–206; c) C. Lee, W. Yang, R. G. Parr, *Phys. Rev. B* **1988**, *37*, 785.
24. a) W. R. Wadt, P. J. Hay, *J. Chem. Phys.* **1985**, *82*, 284–298; b) L. E. Roy, P. J. Hay, R. L. Martin, *J. Chem. Theory Comput.* **2008**, *4*, 1029–1031.
25. a) M. Cossi, G. Scalmani, N. Rega, V. Barone, *J. Chem. Phys.* **2002**, *117*, 43–54; b) V. Barone, M. Cossi, J. Tomasi, *J. Chem. Phys.* **1997**, *107*, 3210–3221.